Arctic Sea Surface Determination with Combined CryoSat-2 and ICESat-2 Data

Guodong Chen[1,2], Weiping Jiang[3], Zhijie Zhang[1,2], Taoyong Jin[4,5], Dawei Li[4,5]

[1]School of Geography Science and Geomatics Engineering, Suzhou University of Science and Technology, Suzhou, 215009, China

5

[2]Suzhou Laboratory, Suzhou, 215009, China

[3]GNSS Research Center, Wuhan University, Wuhan, 430079, China

[4]School of Geodesy and Geomatics, Wuhan University, Wuhan, 430079, China

[5]Hubei Luojia Laboratory, Wuhan, 430079, China

10

Correspondence to: Guodong Chen (cgdtt@126.com)

Abstract. Due to the presence of sea ice, determining the sea surface height in the Arctic Ocean remains a significant challenge. State-of-the-art Arctic Mean Sea Surface (MSS) products are primarily derived from radar altimetry missions like CryoSat-2. However, the ICESat-2 laser altimeter can offer valuable sea surface observations up to 88°N latitude with

15 unprecedented precision and spatial resolution. This paper analyses the performance of combined CryoSat-2 and ICESat-2 data in determining the Arctic sea surface. Comparisons of overlapping observations from both missions reveal excellent consistency, with an inter-mission bias of less than 1 cm in the Arctic. Different geophysical corrections are considered, and the results suggest that only the ocean tide correction needs to be unified, while other corrections show minimal discrepancies. The MSS derived from combined data boasts both superior spatial coverage and precision compared to

20 individual missions. The impact of summer melt pond is also discussed. The data from June, July and August are seriously contaminated, but only have limited effect on the mean sea surface calculation. Overall, the combined use of CryoSat-2 and ICESat-2 data offers a promising approach to accurately determining the Arctic sea surface, paving the way for improved understanding of sea level change and its implications in this critical region.

1 Introduction

25 The Arctic Ocean serves as a critical source of cold water, making it a vital component of global climate system. Understanding Arctic sea surface is crucial for various scientific and practical applications, such as climate studies, resource exploration and voyage safety. However, sea ice impedes direct satellite measurement of the sea surface, while the remote location and harsh environment limit in situ data collection in the Arctic. For altimeters, the Arctic sea surface can be only captured over the large openings between sea ice floes, known as leads. With the advent of the technology that distinguishes

30 measurements over leads from those over sea ice, the Arctic sea surface height was observed by ERS-1 and ERS-2 satellite

altimeters (Laxon et al., 2003), and the first map of Arctic Mean Sea Surface (MSS) was published the next year (Peacock and Laxon, 2004). Since then, satellite altimetry became the primary method for Arctic sea surface height (SSH) studies.

Before 2010, the two most commonly used altimetry missions in Arctic Ocean were ICESat (Forsberg and Skourup, 2005) and Envisat (Connor et al., 2009). However, Envisat data only covered the region south of 81.5 °N, leaving huge gap in

35 Arctic Ocean. While ICESat's reach extended to 86 °N, its operations were limited to just 2-3 months annually during its 7-year lifespan, resulting in intermittent time coverage. Despite these disadvantages, the two missions provided valuable data for Arctic SSH in the first decade of the 21st century (Kwok and Morison, 2011; Farrell et al., 2012; Prandi et al., 2012). With the launch of CryoSat-2 in 2010, the Arctic sea surface research went into a flourishing period. Key problems in polar sea surface determination have been carefully analyzed (Ricker et al., 2014; Wernecke and Kaleschke, 2015; Yi et al., 2018;

40 Xia and Xie, 2018) , and new approaches to radar altimetry data processing have been introduced (Kurtz et al., 2014; Jain et al., 2015; Poisson et al., 2018; Passaro et al., 2018; Lee et al., 2018). As a result of the accumulation of nearly 20 years of altimetry data, the Arctic sea level changes (Cheng et al., 2015; Andersen and Piccioni, 2016; Rose et al., 2019; Lawrence et al., 2021) and sea surface variations (Armitage et al., 2016; Xiao et al., 2020; Bagnardi et al., 2021; Doglioni et al., 2022) can also be inspected at different scales. Currently, Arctic sea surface products are primarily derived from radar altimetry

45 missions, with the majority of data coming from the CryoSat-2 satellite (Prandi et al., 2021; Andersen et al., 2023; Schaeffer et al., 2023), while other recently launched altimetry missions, such as Sentinel-3 and SARAL/AltiKa are also used to extend the Arctic sea level record (Lawrence et al., 2021; Prandi et al., 2021).

The latest laser altimetry mission, ICESat-2, also provides height measurements up to 88 °N and shows promising potential for polar sea surface determination (Kwok et al., 2019; Farrell et al., 2020; Bagnardi et al., 2021; Liu et al., 2023). However,

50 ICESat-2 data have not been utilized in any officially published Arctic sea surface products yet. Some studies also suggested that there may be systematic errors in laser altimetry and radar altimetry in the Arctic Ocean (Kim et al., 2020). Therefore, it is necessary to investigate whether ICESat-2 and CryoSat-2 data can be merged for sea level research in the Arctic Ocean. In this paper, we combine CryoSat-2 and ICESat-2 data for the determination of Arctic SSH, aiming to improve the accuracy and spatial resolution of sea surface measurements. The paper is structured as follows: Section 1 provides a concise

55 overview of existing studies on Arctic SSH determination. Section 2 details the datasets employed in this research. Section 3 introduces the methodology used for calculating Arctic SSH and the results are presented in Section 4. Section 5 delves into the impacts of geophysical corrections and summer melt ponds on SSH determination. Finally, Section 6 summarizes the key findings and contributions of this research.

2 Data description

60 ### 2.1 CryoSat-2 data

CryoSat-2, one of the European Space Agency (ESA) Earth Explorer program missions and dedicated to polar observations, was launched on April 8th, 2010. The satellite and instruments on-board were designed to operate at least three and a half

years with an orbit inclination of 92 ° and altitude of 717 km. However, its innovative design and dedicated operators have kept it in service for over 13 years and counting. CryoSat-2 carries a Ku-band radar altimeter named SIRAL (SAR/Interferometric Radar Altimeter). SIRAL can operating in three modes to handle with different ground surface types. The Low-Resolution Mode (LRM) provides conventional pulse-limited altimetry over open oceans and ice sheet interiors, while Synthetic Aperture Radar (SAR) mode provides smaller footprints over sea ice. Finally, SAR Interferometry (SIN) harnesses two antennas to measure the difference in arrival times between echoes, enabling detailed mapping of complex terrains like mountains and ice sheet margins (Wingham et al., 2006). In this research, SAR mode Level-1b waveform product was used so that the retracking technique and surface type classification can be implemented. To ensure temporal alignment with ICESat-2 data, data from October 2018 to October 2022 was utilized. Access to CryoSat-2 products is readily available through the ESA website (https://earth.esa.int/eogateway/catalog/cryosat-products).

2.2 ICESat-2 data

The Ice, Cloud and land Elevation Satellite-2 (ICESat-2), successor to ICESat, was launched on September 15, 2018, from Vandenberg Air Force Base. Led by the National Aeronautics and Space Administration (NASA), this satellite carries a single, cutting-edge instrument: the Advanced Topographic Laser Altimeter System (ATLAS), a photon-counting laser altimeter, which maps Earth's surface with exceptional precision. Operating at an orbit inclination of 92 ° and an altitude of 500 km, ICESat-2 achieves extensive spatial coverage, reaching up to 88 ° latitude in both hemispheres. One of the primary scientific objectives for ICESat-2 is to estimate sea ice thickness in polar oceans to study the ice/ocean/atmosphere exchanges of energy mass and moisture. This task requires the estimation of sea ice freeboard first, which is determined by the sea surface and sea ice height. Compared with its predecessor, ICESat-2 boasts a significantly smaller footprint and higher spatial resolution, which enhances sea ice freeboard and thickness retrievals (Markus et al., 2017). ICESat-2's along-track sea ice and SSH data can be achieved in the ATL07 product. In this product, each segment within this product represents an average height derived from approximately 150 surrounding laser photon reflections, resulting in a variable along-track resolution ranging from several meters to tens of meters (Kwok et al., 2019). By the time of the beginning of this research, Release 005 was the latest version of ATL07. Consequently, ATL07 Release 005 product is used in this paper, spanning October 14th, 2018 to October 12th, 2022. The dataset can be accessed through the National Snow and Ice Data Center (NSIDC) website (https://nsidc.org/data/icesat-2/data).

2.3 Other data

Some auxiliary datasets were also used in this research. DTU21 MSS model developed by Technical University of Denmark (DTU; Andersen et al., 2023) was used as reference sea surface in altimetry data processing. CNES_CLS 2022 MSS model developed by Centrale Nationale d'Etudes Speciales (CNES; Schaeffer et al., 2023) was used to evaluate the Arctic sea surface calculated in this paper. Monthly sea level records of six gauge stations from Permanent Service for Mean Sea Level (PSMSL) were used to evaluate our altimetry-derived sea level records. Sea Ice Concentrations from Nimbus-7 SMMR and

95   DMSP SSM/I-SSMIS Passive Microwave Data (DiGirolamo et al., 2022), were used to remove altimetry measurements from open ocean. ERA5 (European Centre for Medium-Range Weather Forecasts Reanalysis v5) global meteorological reanalysis data (Hersbach et al., 2020), FES2014 (Finite Element Solution 2014) global ocean tide model (Lyard et al., 2021), and IERS (International Earth Rotation Service) conventions 2010 (Luzum and Petit, 2012) were used for geophysical corrections.

3 Methods

3.1 CryoSat-2 data procession

In studying Arctic SSH using CryoSat-2 data, there are two key data processing steps: lead detection and retracking algorithm (retracker). Lead detection distiguishes open water leads within the ice cover from inherently higher sea ice observations, crucial for SSH accuracy. The retracking algorithm determines the propagation time of radar pulse and thus the distance between satellite and earth surface and finally the surface height. Compared with sea ice freeboards and thicknesses, different retrackers have more significant impact on the determination of sea surface and sea ice height (Xia and Xie, 2018; Yi et al., 2018).

Both of the lead detection and retracking algorithms had been studied in many researches. In this paper, following Chen et al. (2022), CryoSat-2 leads were identified as observations of PP > 70 and SSD < 3.0, where PP and SSD stands for Pulse Peakiness (Peacock and Laxon, 2004) and Stack Standard Deviation (Wingham et al., 2006) respectively. These thresholds of the two parameters are more stringent compared with the commonly used values (Laxon et al., 2013; Passaro et al., 2018; Rose et al., 2019) and might reject more prospective lead observations. However, this strategy can effectively reduce the quantity of 'misidentified leads' (sea ice observations that are mistakenly identified as leads; Chen et al., 2022) and provides reliable SSH measurements. A primary peak centre of gravity (PP-COG) retracker (Jain et al., 2015) was implemented to acquire better precision over leads. The performance of this retracker was verified to be about 10% better than that of ESA level-2 products over leads (Jain et al., 2015).

3.2 ICESat-2 data procession

3.2.1 Overlapping lead observations

In 2020, ESA adjusted the orbit of CryoSat-2 to periodically align with NASA's ICESat-2 to provide nearly coincident radar and lidar measurements over same areas. This campaign is named as Cryo2Ice, which enables direct comparisons of the two missions and sophisticated study on sea ice by fusing their data. In this paper, coincident and overlapping CryoSat-2 and ICESat-2 lead observations were selected so that the data procession of ICESat-2 can be rigorously validated by comparison with CryoSat-2 data. Near-coincident track pairs were first searched on Cryo2Ice website (https://cs2eo.org/cryo2ice). To alleviate the impact of sea ice drift, a maximum separation time of 3 hours and minimum intersection duration time of 1

minute was restricted. Considering the footprint sizes of the two altimeters, a maximum distance between datasets of 5 km was also required. Consequently, 1331 pairs of near-coincident CryoSat-2 and ICESat-2 tracks were found between May 2020 and October 2022. Then the overlapping lead observations were selected as follows.

1) CryoSat-2 lead observations were selected and processed with the identification and retracking methods described in Section 3.1.

2) Potential ICESat-2 lead observations were selected with different criterions (detailed in Section 3.2.2).

3) Centred around each CryoSat-2 lead observation, a logical observation window was established with a size of 305 m along track and 1650 m across track which matched the footprint size of CryoSat-2 SAR mode (Bouzinac, 2014).

4) To match the spatial resolution and locations of CryoSat-2 observations, all the ICESat-2 lead observations located within the box were averaged. This nominal ICESat-2 observation was considered to be overlapping with its corresponding CryoSat-2 observation.

Figure 1 shows the distributions of overlapping observations used in this paper, with a color bar showing the observation times. The two different altimeters both identified these overlapping observations as leads, providing high confidence they were true lead detections. Finally, the overlapping observations were compared and analysed to study the performance of different ICESat-2 data processions.
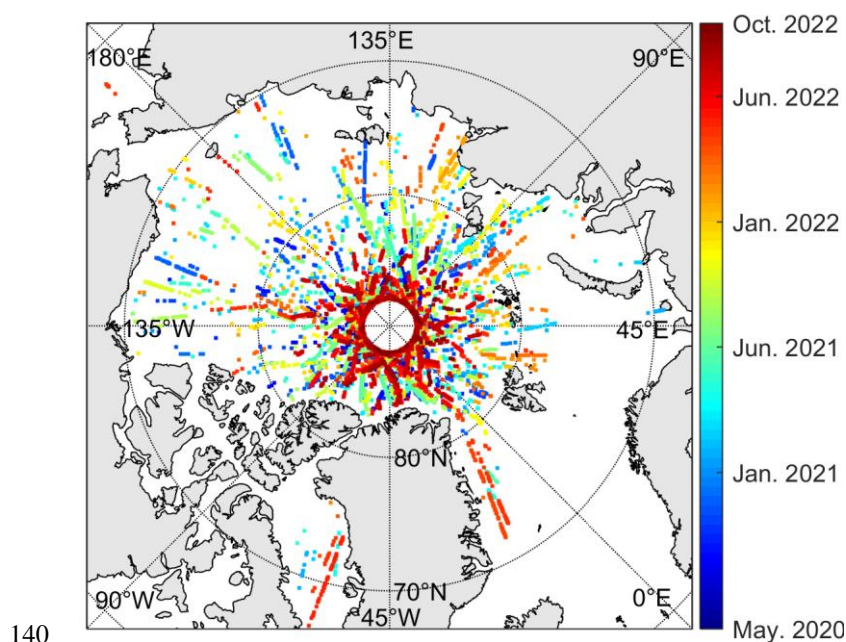

Figure 1: Distribution of overlapping ICESat-2 and CryoSat-2 lead observations.

3.2.2 ICESat-2 beam intensity

ICESat-2 has a single laser split into six beams and arranged in three pairs to better gauge the slope of Earth's surface (Neumann et al., 2019). The separations are 3.3 km between adjacent pairs and 90 m between beams within each pair. Each

145   ICESat-2 beam pair consists of a strong and a weak beam. The energy ratio of the strong and weak beams is approximately 4:1 (Neumann et al., 2019). The relative strength of the left and right beams depends on the observatory orientation of ATLAS, which is adjusted approximately twice per year (Zhang et al., 2022). Obviously, strong beams can provide better signal to noise ratio than weak beams. Therefore, it is reasonable to expect better precision form strong beams under particular circumstances (Zhang et al., 2022), and only observations from strong beams were utilized in some studies

150   (Kacimi and Kwok, 2020; Kwok et al., 2021a; Bagnardi et al., 2021).

  In this section, the influence of beam energy on Arctic sea surface retrieval was evaluated. ICESat-2 measurements that represent sea surfaces were first selected by the height_segment_ssh_flag (abbreviated as SSH Flag hereafter) parameter provided in ATL07 production. A value of 1 of SSH Flag indicates that this measurement is likely reflected by lead (hence represents the sea surface). Then these lead observations were separated into strong and weak beam observations and

155   compared with overlapping CryoSat-2 lead observations following the steps mentioned in Section 3.2.1. The results are summarised in Table 1. The difference with CryoSat-2 of all ICESat-2 observations was also listed for comparison. The mean differences of ICESat-2 strong and weak beams compared with CryoSat-2 are -2.6 cm and 0.4 cm respectively. However, it is difficult to conclude that there is an energy-related bias because of two reasons. Firstly, the 3 cm difference is not large considering the 5-6 cm standard deviations (STD) shown in Table 1. Secondly, other possible effects cannot be

160   excluded according to our results, such as observation time and locations. Therefore, no effort was made to reduce the bias between strong and weak beams in this research. The results shown in Table 1 suggest that the STD of the differences between ICESat-2 weak beams and CryoSat-2 is smaller than strong beams, indicating better consistence. But the values of 5.9 cm and 5.1 cm are still at similar levels. The maximum and minimum differences with CryoSat-2 are also similar, regardless of beam energy. When the strong and weak beams are combined, the differences between ICESat-2 and CryoSat-

165   2 are still at same level, but the number of overlapping observation pairs increased significantly. In conclusion, there is no significant difference between the performances of strong and weak beam observations according to Table 1. Therefore, both strong and weak beams were used in this paper to obtain more ICESat-2 observations.

Table 1: Differences SSH derived from `ICESat-2` strong and weak beams compared with overlapping CryoSat-2 observations

Beam energy	Difference with overlapping CryoSat-2 data				Number of overlapping lead observation pairs
	Mean (cm)	STD (cm)	Max (cm)	Min (cm)	
Strong	-2.6	5.9	30.2	-76.1	26200
Weak	0.4	5.1	31.3	-76.3	19174
All	-1.3	5.6	31.3	-72.6	31507

3.2.3 ICESat-2 lead detection

170   The ATL07 product is generated by analysing the height distributions from geolocated photons using algorithms dedicated to sea ice and open water leads. This product provides two flags for surface type classification: height_segment_type (abbreviated as Surface Type hereafter) and height_segment_ssh_flag (SSH Flag). The former assigns a particular surface

type for each ATL07 height segment according to surface photon rate, width of photon distribution and background rate (Kwok et al., 2019; Kwok et al. 2021a). The Surface Type values of 0, 1, 2-5, 6-9 and -1 indicate cloud covered, non-lead

175 snow/ice, specular lead, dark lead and unknown type respectively (Kwok et al. 2021b). In early releases of ATL07 product, both specular (2-5) and dark lead (6-9) were considered to be possible SSH samples (Kwok et al., 2019). However, clouds can attenuate the strength of the surface returns and lead to similar behaviours of dark leads (Kwok et al. 2021a). Therefore, to prevent misidentification of leads, only specular leads are used for sea surface determination in recent releases (Kwok et al. 2021a; Kwok et al. 2021b). The specular leads are further selected with a post-classification height filtering (Kwok et al.

180 2021a). Only those segments that pass the filtering are marked as SSH segments with a SSH Flag value of 1 and provided as sea surface in other official ICESat-2 products.

To confirm the effect of this lead identification strategy, ICESat-2 observations assigned with different lead types were compared with CryoSat-2, the results are listed in Table 2. Notice that the SSH Flag was not used here, i.e., the height filtering was not implemented. The heights of dark leads (Surface Type = 6-9) are obviously higher than CryoSat-2, which

185 indicates that many non-lead observations were misidentified as leads. This phenomenon can be explained well by cloud attenuation (Kwok et al. 2021a) and suggest that these observations should not be used as SSH measurements unless they can be further classified to reject false leads. Therefore, dark leads were no longer considered in this paper. The specular leads, however, show much better consistence with CryoSat-2. For a Surface Type value of 3-5 (referred to as leads type 3-5 for short), both the mean differences and standard deviations are on the same level of results identified with SSH Flag =1

190 (Table 1). It means these observations were mostly composed of true leads even without the height filtering mentioned by Kwok et al. (2021a). The standard deviation of Surface Type =2 (referred to as lead type 2 for short) shown in Table 2 is similar to dark leads, much larger than other specular leads. The 4.6 cm mean difference is also larger than other specular leads, but smaller than dark leads. These results indicate that false leads can be misidentified when Surface Type was assigned as 2, although not as much as the situation of dark leads.

195 **Table 2: Differences between ICESat-2 leads identified by different height_segment_type values and overlapping CryoSat-2 leads**

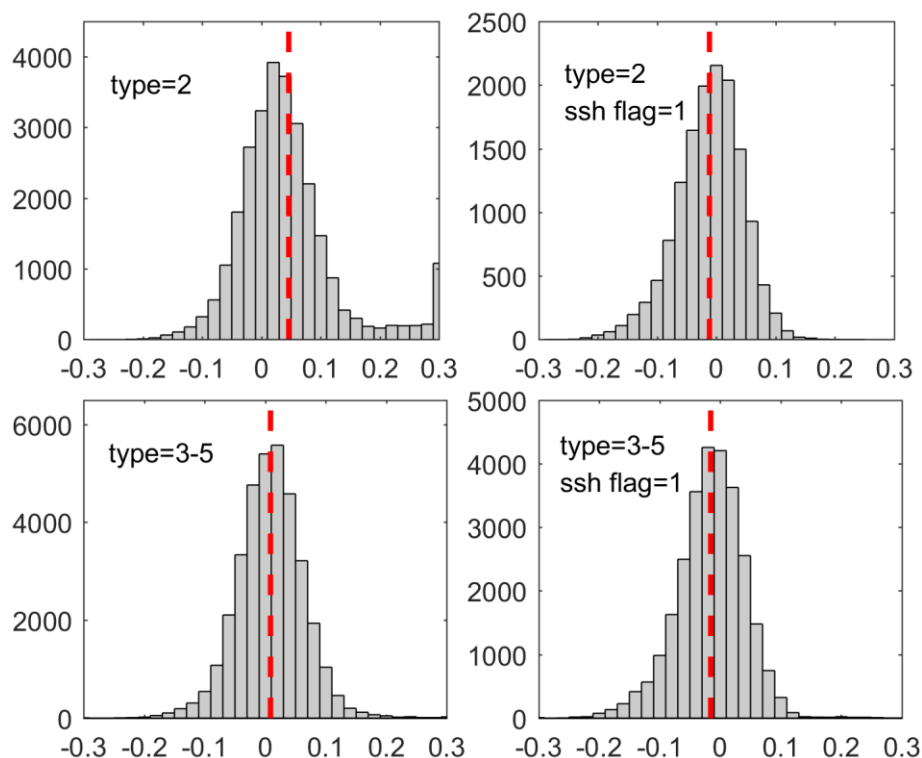| Surface Type	Difference with overlapping CryoSat-2 lead observations				Number of overlapping lead observation pairs
	Mean (cm)	STD (cm)	Max (cm)	Min (cm)	
2	4.6	9.7	78.2	-28.3	28297
3	2.0	5.0	77.4	-44.6	14682
4	0.4	5.9	59.8	-24.4	20388
5	0.6	5.0	57.2	-33.7	10872
6	9.0	8.0	94.2	-27.7	19870
7	12.4	10.5	96.8	-47.1	22500
8	12.8	10.1	91.4	-25.2	13923
9	17.4	12.4	93.6	-32.5	17044

To evaluate the effect of the height filtering procedure, we separated the specular leads into two groups, with Surface Type of 2 and 3-5. Then the two groups were compared with overlapping CryoSat-2 both with and without the constraint of SSH Flag =1. The results and statistical histograms are shown in Table 3 and Fig. 2 respectively. It can be seen from the results that, for specular lead type 2, the constraint of SSH Flag =1 significantly improved the consistency with CryoSat-2, showing the effectiveness of the height filtering procedure. This conclusion can be also confirmed from the histograms: non-normally distributed positive values existed before height filtering (Fig. 2 top left) while disappeared after the procedure (Fig. 2 top right). However, it also reduced the number of observations by half according to Table 3. For specular leads type 3-5, no obvious improvement can be seen after height filtering but the observation number was also reduced. The problem of height filtering is that this procedure rejected not only the false leads but also many true leads that are slightly higher than surroundings due to the observation accuracy of ICESat-2, leading to an underestimate of sea surface. Moreover, underestimates were found over leads in ATL07 product (Liu et al., 2023), which would be probably assigned as sea surface by height filtering due to their lower elevations, while other true leads with normal accuracies would be rejected. This effect can be inferred from the statistics of specular lead type 3-5. The standard deviations are almost the same with and without the SSH Flag constraint, suggesting that the procedure is unnecessary, while the mean difference decreased from +0.9 cm to -1.6 cm. Another evidence can be seen from histograms. The data of specular leads type 3-5 correspond well to normal distribution before height filtering (Fig. 2 bottom left) while skewing-to-negative asymmetries can be seen with the additional constraint (Fig. 2 top and bottom left). Besides, the decline of the quantity of observations is also noteworthy. Low lead fraction in Arctic (Lindsay and Rothrock, 1995) results in sparse SSH measurements from satellite altimeters, therefore, any reductions in observation quantity is unfavourable for Arctic sea surface studies.

Table 3: Effect of SSH Flag for specular leads validated by overlapping observations

SSH Flag	Surface Type	Difference with overlapping CryoSat-2 lead observations				Number of overlapping lead observation pairs
		Mean (cm)	STD (cm)	Max (cm)	Min (cm)	
Not used	2	4.6	9.7	78.2	-28.3	28297
	3-5	0.9	5.5	59.8	-44.6	35256
1	2	-1.2	5.6	24.5	-28.3	14194
	3-5	-1.6	5.6	31.3	-72.6	27507

According to our results, the observations of specular lead types 3-5 have a great consistency with CryoSat-2. The mean differences are close to zero and the histogram conforms to normal distribution, indicating that the main error is consist of accidental errors. The height filtering procedure is not necessary for these observations because it may result in reduction of quantity of observations and underestimats sea surface. For specular lead type 2, however, the height filtering is necessary to reject false leads. Although the results may be lower compared with CryoSat-2, the 1-2 cm bias is acceptable. Therefore, these two types mentioned above were selected as true leads for ICESat-2 data procedure in this research.

Figure 2: Statistical histograms of differences of different specular leads from ICESat-2 compared with overlapping CryoSat-2 data. Red dashed lines indicate mean differences.

3.3 Mean sea surface determination

Before SSH determination, observations over open oceans were rejected with sea ice concentration less than 50% according to Sea Ice Concentrations from Nimbus-7 SMMR and DMSP SSM/I-SSMIS Passive Microwave Data (DiGirolamo et al., 2022). The along track resolution of CryoSat-2 SAR mode is around 305 m while it varies from meters to tens of meters according to photon density for ICESat-2 ATL07 product. Again, to avoid differences caused by spatial resolutions, ICESat-2 leads identified from ATL07 product were separated into 305 m × 1650 m rectangular windows and averaged (mentioned as resampled ICECSat-2 observation for simplicity) to match the resolution of CryoSat-2. Since distances between and within ICESat-2 ground track pairs are 3.3 km and 90 m, the reduced resolution resulted in 3 ground tracks over large leads. The quantities of lead observations of CryoSat-2 and resampled ICESat-2 observations for each month are illustrated in Fig. 3.

The DTU21 MSS model was subtracted as a reference from altimetry observations to obtain SSHA (sea surface height anomaly), so that large scale sea surface variations can be avoid during SSH determination. It can be seen from Fig. 3 that the observation numbers differed between seasons. In summer months (June to August), almost tenfold of leads were found by both altimetry missions compared with other months due to the melting of sea ice (also the presence of melt ponds over

sea ice). Therefore, the mean sea surface was not determined by simply averaging the elevation of the leads in this study. Instead, it was determined by fitting the time series of local monthly averaged SSHA. The Arctic Ocean was divided into 5 km × 5 km grids defined by NSIDC's Northern Hemisphere Polar Stereographic Projection. Lead observations were averaged monthly inside each grid after outlier rejection by 2δ criterion. If there was at least 5 monthly averaged SSHA and the timespan of the time series was no shorter than 2 years, the time series of this grid was linearly fitted with least square adjustment:

$$H(t_i) = H(\bar{t}) + dH/dt \cdot (t_i - \bar{t}) \tag{1}$$

Where t_i is the ith month and $H(t_i)$ is the monthly average SSHA of this month. $\bar{t}$ denotes average time of whole time span of altimetry missions (prescribed as 2021.0 in this paper) while $H(\bar{t})$ represents the mean SSHA of this grid. dH/dt denotes inter-annual sea surface trend.
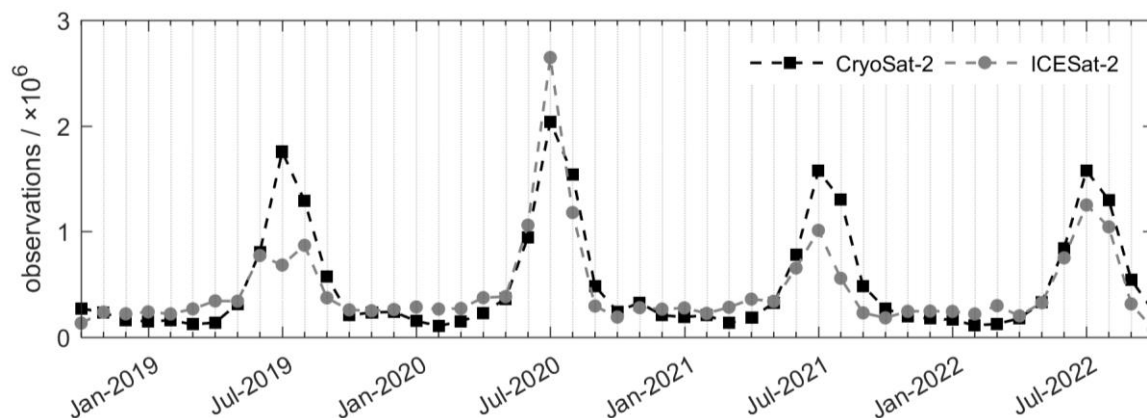

Figure 3: Numbers of CryoSat-2 and ICESat-2 lead observations identified in this paper. Notice the resolution of ICESat-2 had been lowered to match CryoSat-2.

Mean SSHA results were calculated with both individual CryoSat-2/ICESat-2 data and combined data. No interpolation or smoothing techniques were implemented to these gridded mean SSHA so that the true accuracies and spatial distributions of different data sources can be evaluated. Finally, mean SSHA can be restored to mean SSH by adding DTU21 MSS to it.

4 Results

4.1 Arctic sea surface derived from individual CryoSat-2/ICESat-2 data

Arctic mean SSHA (referenced with DTU21 MSS) was first calculated with data from individual mission, so that the performances of CryoSat-2 and ICESat-2 can be evaluated and compared. The results are illustrated in Fig. 4.
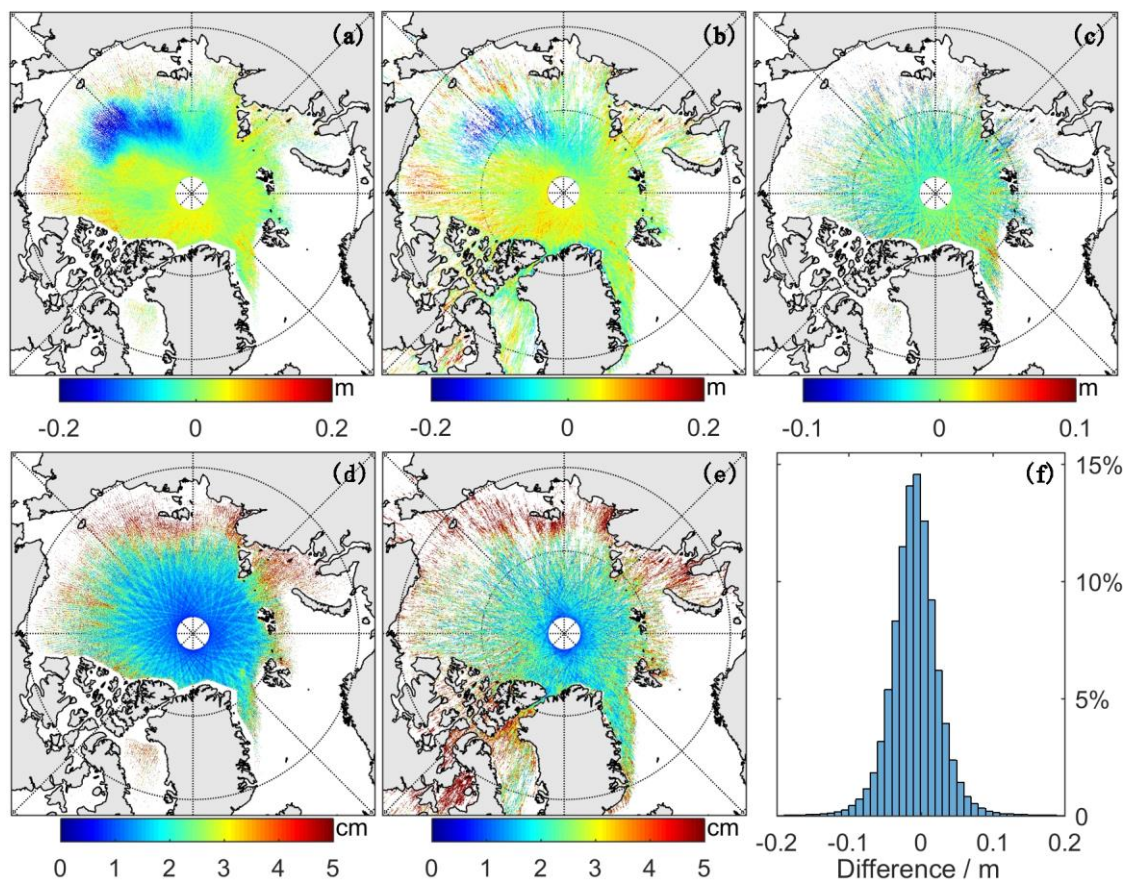
Figure 4: Illustration of (a) SSHA from CryoSat-2, (b) SSHA from ICESat-2, (c) SSHA differences between CryoSat-2 and ICESat-2, (d) RMSE of CryoSat-2 derived SSHA, (e) RMSE of ICESat-2 derived SSHA, and (f) histogram of SSHA differences of the two missions.

265

With the method introduced in Section 3.3, SSHA results of 190041 and 205699 grids were estimated with CryoSat-2 and ICESat-2 data respectively. The former fills less grids because CryoSat-2 SAR mode doesn't operate over coastal regions, leading to blanks around Baffin Bay, Canadian Arctic Archipelago and Greenland, as shown in Fig. 4(a). ICESat-2 provides reasonable results along those coasts in Fig. 4(b), however, its coverage in central Arctic is much sparser compared to

270 CryoSat-2, especially those gaps in Beaufort Sea and East Siberian Sea. This problem indicates that ICESat-2 failed to identify as much leads as CryoSat-2, even though we had utilized more lead segments than official products. This can be also inferred from Fig. 3. Since ICESat-2 observations were resampled and finally resulted in 3 simultaneous ground tracks, it was expected that ICESat-2 resampled lead observations should be about 3 times of CryoSat-2 lead observations, supposing the two altimeters had similar ability of lead identification. However, the quantities of lead observations of the two missions

275 were on the same level all through the time span according to Fig. 3. It is worth mentioning that the CryoSat-2 lead observation quantity shown in Fig. 3 is probably underestimated because our choice of thresholds for CryoSat-2 lead identification was conservative compared with former studies (e.g. Laxon et al., 2013; Passaro et al., 2018; Rose et al., 2019).

Therefore, Fig. 3 and Fig. 4(b) together suggest that substantial lead segments may be missed by the original identification strategy provided in ATL07 product. An advanced identification method is needed, especially for those dark leads.

280   Despite of the different behaviours on data coverage, the two missions show excellent consistency with each other according to Fig. 4(a) and (b). Similar patterns can be found in results of both missions. The differences of the two missions are shown in Fig. 4(c). The mean difference is -0.81±3.52 cm (result of ICESat-2 is higher) recorded from 136559 overlapping grids, the histogram is shown in Fig. 4(f). No obvious spatial pattern can be found in Fig. 4(c) and Fig. 4(f) conforms well to normal distribution. These results prove that both CryoSat-2 and ICESat-2 can provide reliable sea surface in Arctic Ocean.
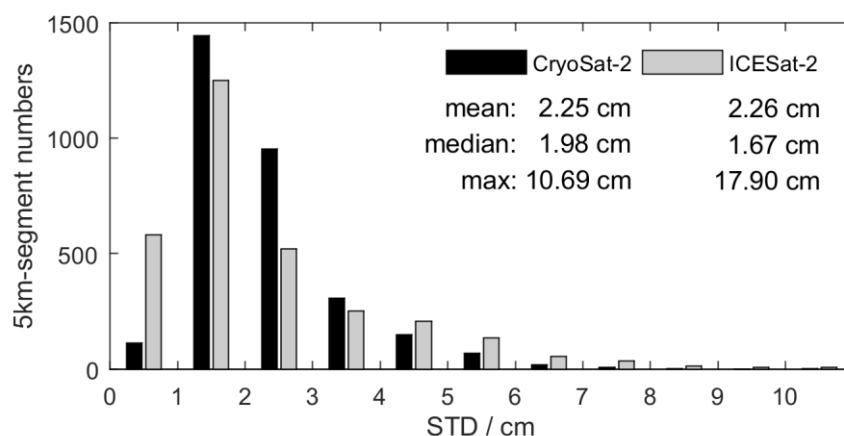
285

Figure 5: Histograms of standard deviations in 5 km along track segment SSHA of CryoSat-2 and resampled ICESat-2 measurements

Figure 4(d) and (e) illustrate the RMSE in each grid for Fig. 4(a) and (b). Basically, the two figures show similar patterns, smaller RMSE appear in central Arctic due to converged tracks while it became larger toward the coasts. Within the

290   overlapping regions displayed in Fig. 4(c), the median RMSE for CryoSat-2 and ICESat-2 were 1.60 and 2.05 cm respectively. The outliers among the results of the two missions were similar. For CryoSat-2, the quantities of unreliable grids with SSHA exceeding ±0.2 m or inter-annual sea level change rate exceeding 0.1 m/a were 134 and 388 while for ICESat-2 the numbers were 117 and 444. However, the RMSE after adjustment in each grid was affected not only the precision of altimeter measurements but also the number of observations and sea surface variations over time. To better

295   understand the precision of the two satellite missions, the overlapping lead observations in Section 3.2.1 were divided into 5 km along track segments and standard deviations (STD) of SSHA were inspected. Within each 5 km segment, CryoSat-2 and resampled ICESat-2 measurements were first detrended by linear fitting to remove the residuals of geophysical corrections, then the standard deviations of the two missions were calculated. To avoid errors caused by small sample sizes, only segments containing at least 5 pairs of overlapping observations were counted. 3065 segments were finally inspected and the

300   histograms of along track STDs are shown in Fig. 5. Again, the two missions show close mean values of STD of 2.25 and 2.26cm, but different features of histograms and statistics can be revealed. The mean and median values of CryoSat-2 are closer, indicating less gross errors. More than 88% of the STD of CryoSat-2 concentrates in the range of 1-4 cm, and only 8

segments emerged STDs over 7 cm. The amount of ICESat-2 segments with STD less than 1 cm is much more than that of CryoSat-2, leading to a smaller median STD (1.67 cm) compared with CryoSat-2 (1.98 cm). However, ICESat-2 also has

305   more segments with larger STD. 64 segments emerged STDs over 7 cm for ICESat-2, that is 8 times of CryoSat-2. According to these results, ICESat-2 has more potential in precision than CryoSat-2 but its performance is not as stable as the latter. A possible explanation may be the sensitivity to atmospheric condition of laser altimeter: ICESat-2 can achieve excellent precision under ideal atmospheric conditions while outliers appear due to poor penetration of laser beams if mist, fog or thin cloud is present. Generally, all these facts above seem to indicate that the two missions have comparable

310   precisions in Arctic sea surface determination.

4.2 Arctic sea surface derived from combined CryoSat-2 and ICESat-2 data

Before combining data from the two missions, the inter-mission bias between CryoSat-2 and ICESat-2 should be removed. Crossover adjustment can be used to analysis biases between multi-missions in mid and low latitude oceans (Jin et al., 2016), but it is not practicable in Arctic Ocean due to the scarcity of leads. Instead, the differences of the gridded monthly averages

315   of the two missions were investigated, the results are shown in Fig. 6. The mean difference of the whole time span was -0.73±1.37 cm (result of ICESat-2 is higher) and no significant long-term trend or seasonal signals can be found in Fig. 6. The -0.73 cm mean difference is close to the mean difference shown in Fig. 4(f). Therefore, a fixed correction of -0.73 cm was applied to resampled ICESat-2 measurements to alleviate the bias between the two missions.
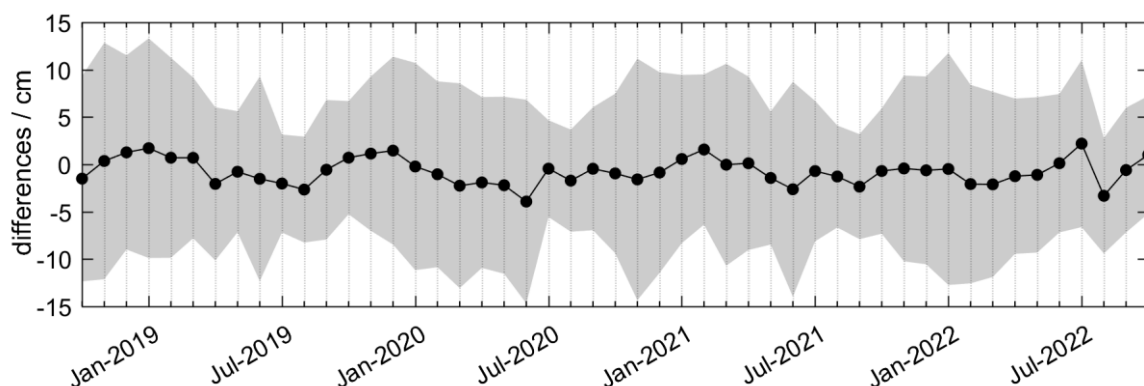

320   **Figure 6: Differences between monthly averaged Arctic sea surface derived from individual CryoSat-2 and ICESat-2. Black dots and solid lines show mean differences and gray area represents standard deviations.**

Mean Arctic sea surface height between October 2018 and October 2022 was then calculated with combined CryoSat-2 and ICESat-2 data, following the procedures introduced in section 3.3. The results are shown in Fig. 7. As expected, the coverage of the results derived from combined data was better than the results from individual missions. Sea surface heights and sea

325   level variation trends of 304449 grids were estimated, while the numbers were 190041 and 205699 in Fig. 4(a) and (b), about 2/3 of the combined data. Fig. 7(a) illustrates the spatial distribution of mean SSHA and Fig. 7(b) shows the mean SSH by adding DTU21 MSS back. For simplicity, the sea surface heights derived from combined CryoSat-2 and ICESat-2 data are

referred as CI-SSHA/SSH hereinafter. The median length of monthly average SSHA time series in each grid derived from combined data was 18 months, while it was 13 and 8 months for individual CryoSat-2 and ICESat-2. Due to increased

330 observation quantity, the RMSE of CI-SSHA, as shown in Fig. 7(d), is also improved. The median value is 1.37 cm in Fig. 7(d).
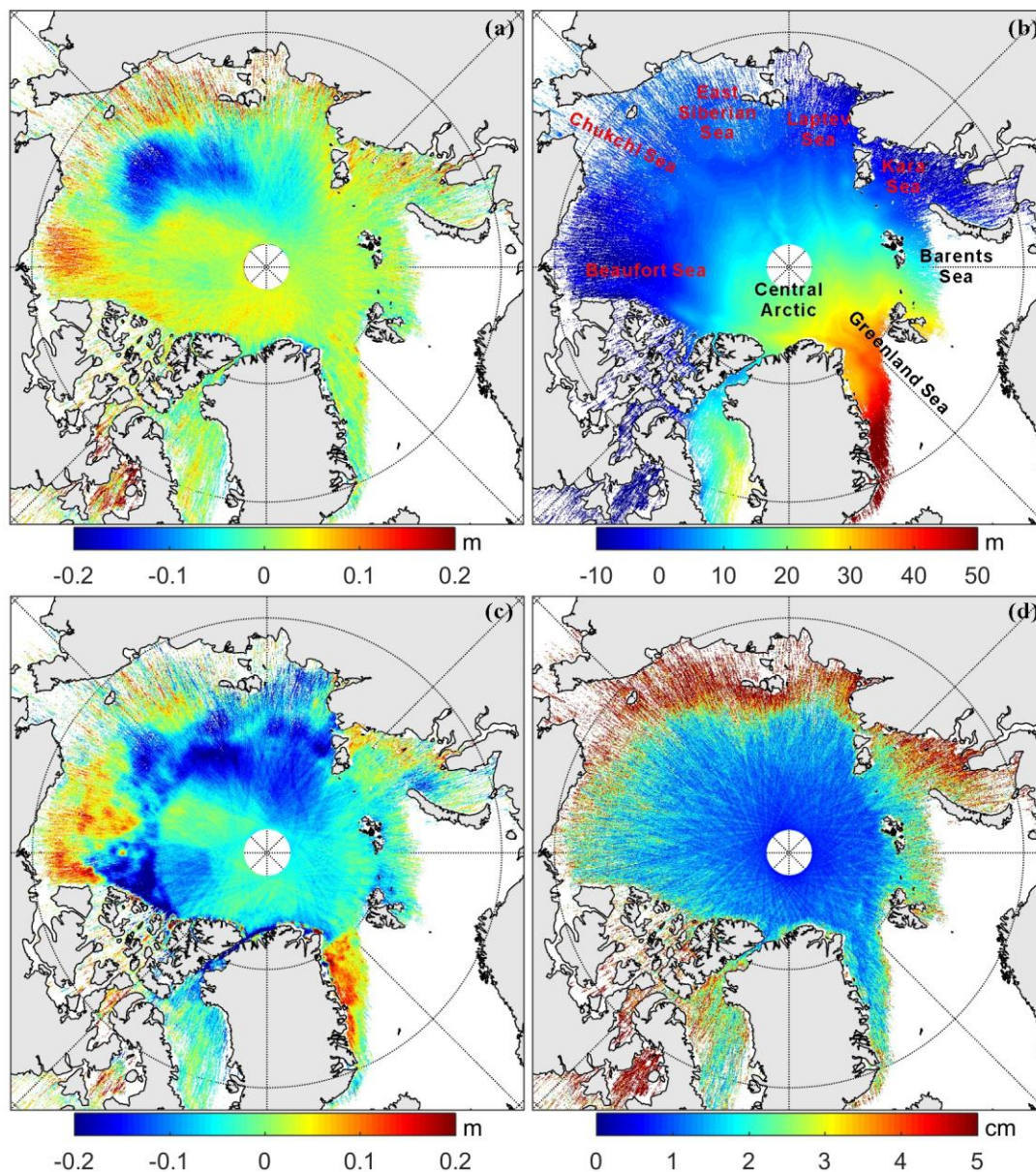

Figure 7: Results of mean sea surface determination with combined CryoSat-2 and ICESat-2. (a) SSHA (referenced with DTU21 MSS) map, (b) SSH map, (c) differences between (b) and CLS2022 MSS (d) RMS of derived SSHA.

335   Since CI-SSHA is referenced with DTU21 MSS model, Fig. 7 (a) can also be regarded as the differences between CI-SSH and DTU21 MSS. The distributions of CI-SSHA are continuous in most of the region even though no filtering was implemented in our procedure. The mean difference is 0.84±6.81 cm. Small-scale features of Arctic mean SSH can be clearly seen in Fig. 7(b), such as Lomonosov Ridge and the Chukchi Plateau (Schaeffer et al., 2023). CI-SSH is also compared with another widely used model, CNES_CLS 2022 MSS, as shown in Fig. 7(c). The mean difference is -4.04±8.28

340   cm. Discontinuities can be seen from Fig. 7(c), especially the circle near 82°N, which is probably due to the different data sources of CNES_CLS 2022 MSS below and above the latitude. It is not surprising that there are regional differences between MSS models due to different data sources and processions. As a comparison, the mean difference between DTU21 and CNES_CLS 2022 was -4.88±6.92 cm within the same region of Fig. 7.

The accuracies of CI-SSHA/SSH are difficult to be quantitatively evaluated because the two best altimetry missions have

345   already been used. Therefore, leads from CryoSat-2 between July 2010 and September 2018 were used for validation of CI-SSH and the two MSS models. Almost 5 billion CryoSat-2 lead observations were selected for SSH validation following the lead identification method introduced in Section 3.1. These validation data, however, is not independent from all three Arctic SSH result or models. CryoSat-2 data of this period was used in DTU21 and CNES_CLS 2022 model constructions, and the lead identification method was the same as CI-SSH. Therefore, the results of this validation cannot present the actual

350   precisions of the SSH results but can only be served as a reference. The differences were -2.11±15.41cm for CI-SSH, -1.63±15.34cm for DTU21 and -7.76±15.62cm for CNES_CLS 2022 within the common coverage of the three SSH results. Although CI-SSH was constructed with data of only 4 years from two altimetry missions, it shows similar performance with the two meticulously constructed SSH models, which shows the great potential of combined CryoSat-2 and ICESat-2 data in Arctic sea surface determination.

355   **4.3 Arctic sea level changes**

Since the time series of monthly average SSHA in each grid is established, the Arctic sea level changes can be revealed. Seasonal (three-months-averaged) SSHA maps in sea ice covered regions are illustrated in Fig. 8. Due to the large cross track distance and sparse lead distribution for each month, the results were interpolated and filtered by a 150-km radius Gaussian filter for better illustration. Some seasonal features can be revealed from Fig. 8, such as the strong negative SSHA

360   signal between Chukchi Sea and East Siberian Sea in spring, and the rise of SSHA in Beaufort Sea and around Russian Coasts in winter. The inter-annual sea level trend can also be estimated by solving formula (1), the results are shown in Fig. 9, along with RMSE. The sea level trends during October 2018 and October 2022 were totally different from the trend of earlier period (Carret et al., 2017; Rose et al., 2019). The two most eye-catching characteristics of Fig. 9(a) are the strong negative signal in Beaufort Gyre and the massive positive signal in multi-year sea ice region north of Greenland and

365   Canadian Arctic Archipelago. These signals may be attributed to the variation of liquid freshwater content (Wang, 2018) due to the weakening of Beaufort Gyre (Lin et al., 2023) and the decline of sea ice (Petty et al., 2023).
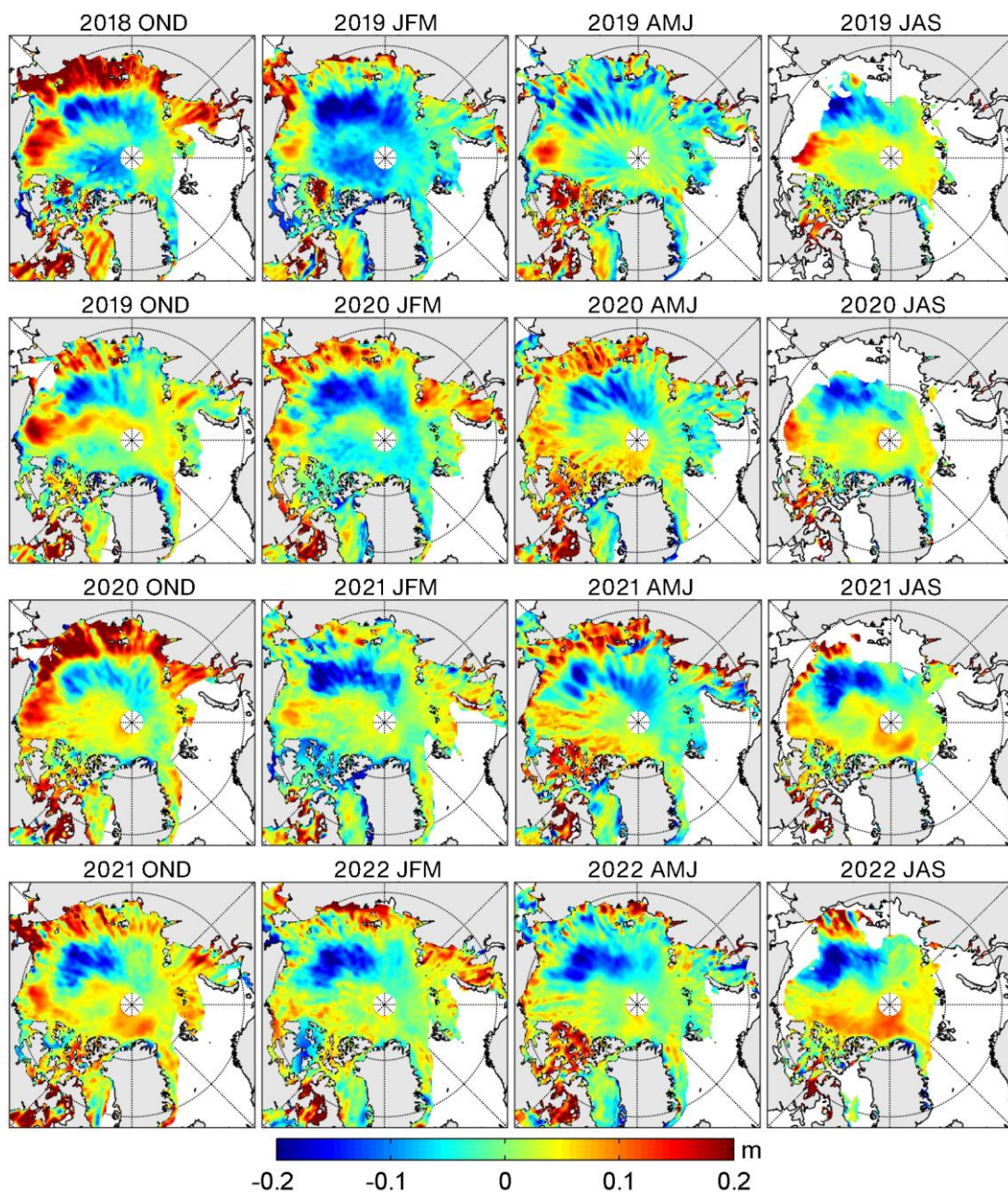
Figure 8: Seasonal average SSHA from October 2018 to October 2022, referenced with DTU21 MSS. OND represents October, November, December; JFM represents January, February, March; AMJ represents April, May, June; JAS represents July, August, September.

Due to the scarcity of polar data, it is difficult to precisely verify our SSH change results mentioned above. Instead, the altimetry-derived time series was quantitatively evaluated with monthly mean sea level data measured by 6 tide gauges. These tide gauge records were provided by PSMSL (Permanent Service of Mean Sea Level) and the location of the 6 tide

gauges are marked in Fig. 9(a). In Arctic, tide gauges are rare since Russian closed most of their tide gauges in 1990s, and

375 the records of many tide gauges are discontinuous in time. The 6 tide gauges in Fig. 9(a) were the best ones we can find. Only one particular tide gauge, the one at Prudhoe Bay, had complete monthly time series between October 2018 and October 2022, while the other 5 tide gauges had at least 27 months of sea level records of the entire time span. The altimetry records were calculated by the average value of all grid points within a radius of 50 km around each tide gauge. Since the datums of gauge and altimetry data are different, both data sets were normalized by reducing the mean sea level before

380 comparison. The final results are illustrated in Fig. 10, the discontinuity of altimetry records can be attributed to the sea ice free periods in summers, because both ICESat-2 and CryoSat-2 data in this paper were clipped by sea ice concentration. Both sea level time series of tide gauge and altimetry show similar patterns in most situations, proving that the altimetry records can generally capture the seasonal and inter-annual variation of Arctic sea level. The correlation coefficients between gauge and altimetry data of each gauge station are listed in the bottom right corners in each subfigure. The best correlation

385 coefficient of 0.79 was obtained in Kotelnyi station while the least value of 0.51 showed up in Tuktoyaktuk station. The overall correlation coefficient for all the 6 stations was 0.64. Minor differences are expected because both data sets were not carefully calibrated and gauge data are more sensitive to runoffs of inland rivers. It should be noted that the length of monthly mean sea level time series was too short for the comparison with gauge data when individual CryoSat-2 or ICESat-2 data was used, due to much less observations compared with the combined data.
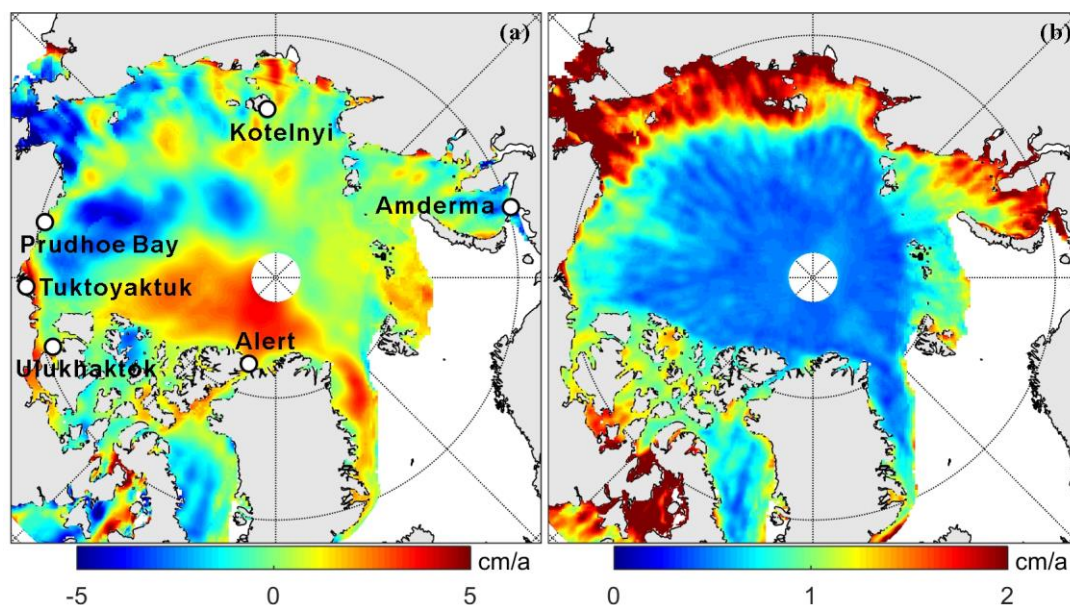
390

Figure 9: Average Arctic sea level change (a) between Oct. 2018 and Oct. 2022 and the corresponding RMSE (b). The white circles in (a) represents locations of the selected tide gauge stations.

17
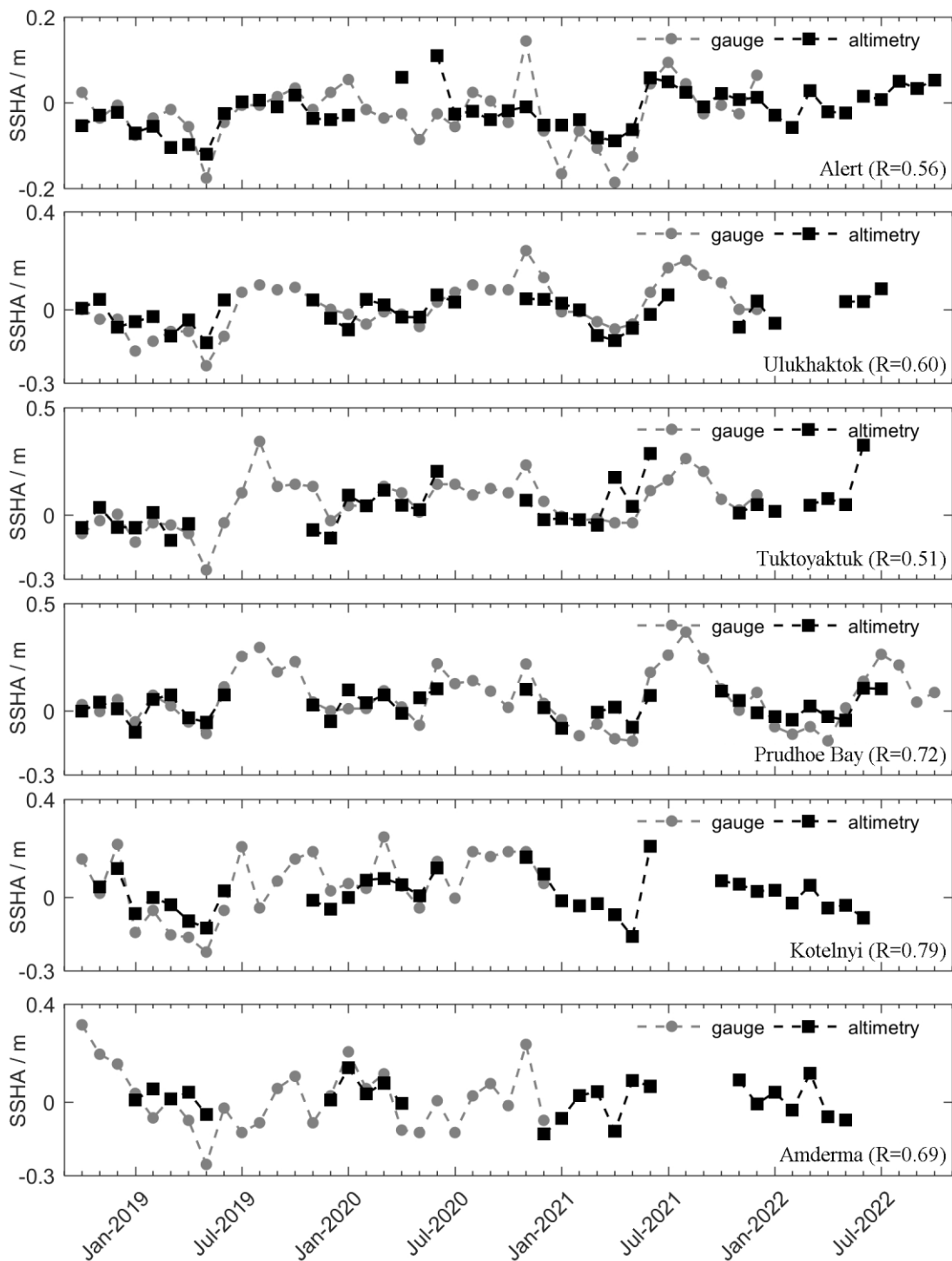
Figure 10: Sea level time series established by tide gauge records (grey dots) and altimetry data (solid square), the tide gauge

395 **station names are listed in the bottom right corners, values in the brackets represent the correlation coefficients between the two**

data.

5 Discussion

5.1 impact of geophysical corrections

Geophysical corrections of altimetry data are essential for sea surface determination, especially with combined multi-mission

400 datasets (Quartly et al., 2019). Usually, unified correction methods are beneficial for the combination of different data source. However, due to the obstruction of sea ice and the scarcity of polar data, the accuracy of the geophysical correction model in the Arctic Ocean is not sufficient (Ricker et al., 2016; Rose et al., 2019). Different geophysical correction models are applied in CryoSat-2 and ICESat-2 products. These corrections can be compared by overlapping lead observations introduced in Section 3.2.1 to determine whether unified models are needed for geophysical corrections for the two satellites. Six

405 geophysical corrections that have directly effect on the variation of sea surface are analysed here, including inverse barometric effect, ocean tide, long-period equilibrium tide, ocean load tides, solid earth tide, and geocentric pole tide. Errors that only affect the range measurement of the altimeter, such as atmospheric delay correction, are not considered. The models/data sources for geophysical corrections applied in the two satellite products, along with their differences are listed in Table 4. It should be noted that the values in Table 4 represents not only the differences caused by correction models but also

410 the sea surface changes due to the observation time differences (less than 3 hours). According to Table 4, the differences in the three corrections of long period equilibrium tide, ocean load tide, and geocentric pole tide in the two satellite products are negligible, which is consistent with the results of Bagnardi et al. (2021). Considering the range error of centimetres to decimetres over leads for satellite altimetry (Jain et al., 2015; Kwok et al., 2021a), the 1-2 mm difference can be ignored. In other words, whether or not unifying these three corrections will not have substantial impacts on the combination of

415 CryoSat-2 and ICESat-2 in Arctic sea surface determination.

Table 4 Models or data sources applied for geophysical corrections in CryoSat-2 and ICESat-2 products and their differences.

Geophysical corrections	Model/Source		Difference (cm)	
	CryoSat-2 （Bouzinac, 2014）	ICESat-2 （Kwok et al., 2021b）	Mean	STD
Inverted barometer effect	Meteo France	MOG2D	-2.1	1.2
Ocean tide	FES2004	GOT4.8	-0.2	7.8
Long period equilibrium tide	FES2004	GOT4.8	0.0	0.2
Ocean loading tide	FES2004	GOT4.8	0.0	0.2
Solid earth tide	Cartwright model	IERS Conventions 2010	-0.1	0.9
Geocentric polar tide	Wahr model	IERS Conventions 2010	0.0	0.1

The corrections for inverse barometer effect, ocean tide, and solid earth tide of the two products differ significantly. The FES2004 and GOT4.8 tide models are applied for CryoSat-2 and ICESat-2 respectively. Their mean difference is only -0.2 cm, but the STD is as high as 7.8 cm, show largest discrepancy among six geophysical corrections. The average difference

420 caused by inverse barometric correction was -2.1±1.2 cm. The mean difference of -2.1 cm is the largest bias in Table 4, indicating that there is an obvious systematic difference between the two data sources. The average difference caused by the solid earth tide correction of -0.1±0.9 cm is not as large as the above two, but it is still a large difference compared to long period equilibrium tide, load tide, and pole tide corrections. To understand the actual effect of model differences on altimetry data accuracy, the original values of the above three corrections applied in CryoSat-2 and ICESat-2 products were replaced

425 with corrections derived from unified models. ERA5 (European Centre for Medium-Range Weather Forecasts Reanalysis v5) global meteorological reanalysis data (Hersbach et al., 2020), FES2014 (Finite Element Solution 2014) global ocean tide model (Lyard et al., 2021), and IERS (International Earth Rotation Service) conventions 2010 (Luzum and Petit, 2012) were used for inverted barometer effect correction, ocean tide correction and solid earth tide correction respectively. Table 5 lists the discrepancies that arise in overlapping altimetry data when each of the three aforementioned corrections is applied

430 individually, while the other two maintain their original values. According to Table 5, the mean difference between the two altimetry data was reduced when unified FES2014 tide model was used for ocean tide correction. The mean difference is closer to zero (from -0.69 cm to -0.46 cm) and the STD decreases by about 0.5 cm (from 5.61 cm to 5.10 cm), compared with original corrections. Therefore, a unified ocean tide model is necessary when combining CryoSat-2 and ICESat-2 in Arctic Ocean. When unified solid earth tide correction was applied, the difference between the two satellite was not

435 improved, indicating that the accuracies of original solid earth corrections were on the same level. When unified inverse barometer correction was applied, the mean difference increased by about 2 cm (from -0.61 cm to -2.69 cm), which is consistent with the conclusion in Table 4. The STD of the difference only increased by 0.01 cm. This indicates that the difference between original inverse barometric corrections in the two missions is mainly emerged as systematic bias, and there is no significant difference in the correction effects. Therefore, it is unnecessary to use unified inverse barometer

440 correction or solid earth correction unless new models with better accuracies in Arctic were published.

Table 5: Differences between overlapping ICESat-2 and CryoSat-2 lead observations when different inverse barometer effect, ocean tide and solid earth tide models were applied.

Geophysical corrections	Differences between CryoSat-2 and ICESat-2 (cm)			
	Min	Max	Mean	STD
With original corrections	-59.3	44.9	-0.61	5.61
With inverse barometer corrections derived from ERA5	-62.0	42.2	-2.69	5.60
With ocean tide corrections derived from FES2014	-56.5	28.3	-0.46	5.10
With solid earth tide corrections derived	-59.1	44.4	-0. 62	5.62

from IERS conventions 2010

5.2 Impact of summer melt ponds

445 As summer temperatures rise, melting snow and ice accumulate on the sea ice surface, leading to formation of melt ponds. Both radar and laser altimeters have difficulties in distinguishing the melt ponds from open leads (Lee et al., 2018; Tilling et al., 2020). Altimetry observations over these melt ponds, which are obviously higher than local sea surface, introduce substantial bias into sea level determinations. It is also reported that these melt ponds lead to an underestimation of sea ice elevation derived from CryoSat-2 (Dawson and Landy, 2023).
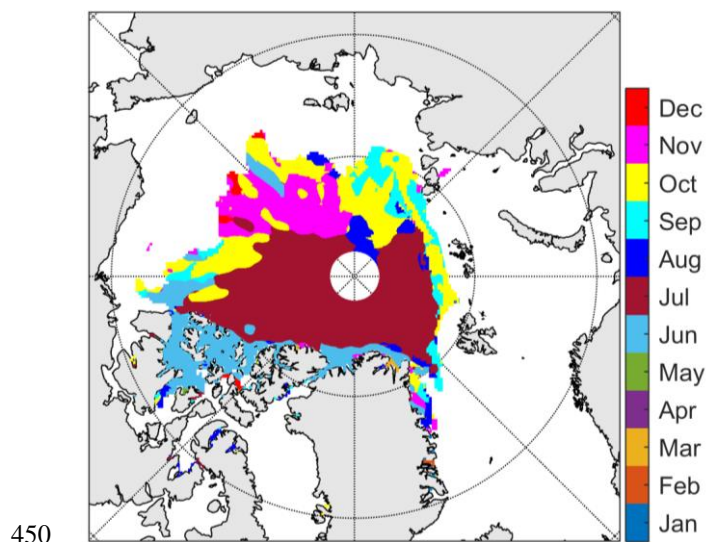
450

Figure 11: Map of peak month of sea surface seasonal cycle revealed with altimetry data, which represents the months when the sea level reaches its annual maximum with different colors.

As shown in Fig. 3, the amount of "lead" observations in June-August is anomalously large for both CryoSat-2 and ICESat-2, especially in July, which can be tens of times the amount of winter months. These three months are also the warmest three

455 months of the year in Arctic, with average temperatures typically above 0°C in recent years. Based on current understanding of Arctic sea ice leads (Lindsay and Rothrock, 1995; Stroeve et al., 2014; Zhang et al., 2018), the amount of observations in summer shown in Fig. 3 is difficult to be trusted. Instead, it is more likely that altimetry data are contaminated by numerous melt pond observations. Figure 11 shows the month when the peak of the seasonal cycle of sea level appears in each 5 km grid. In central Arctic, where the ocean is covered by sea ice all year round, the months of sea level peaks revealed by

460 satellite altimetry are almost all July. This result is inconsistent with the conclusion of Armitage et al. (2016) that the sea level peaks in the Arctic Ocean generally occurs in October-November. Since their study also utilized a large amount of observations from open ocean, which was less affected by melt ponds, we believe their conclusion is more reliable. Furthermore, we checked the monthly average SSHA (referenced with CI-SSH) from June to August in 2019-2022, as

21

shown in Fig. 12. There are abnormal rises in sea level every June-August, with July being the most severe. These rises are
465   generally concentrated in central Arctic, where sea ice is thicker. All of these phenomena indicate that the sea level derived
from altimetry in the Arctic Ocean in summer months, especially in July, can be seriously affected by melt ponds.
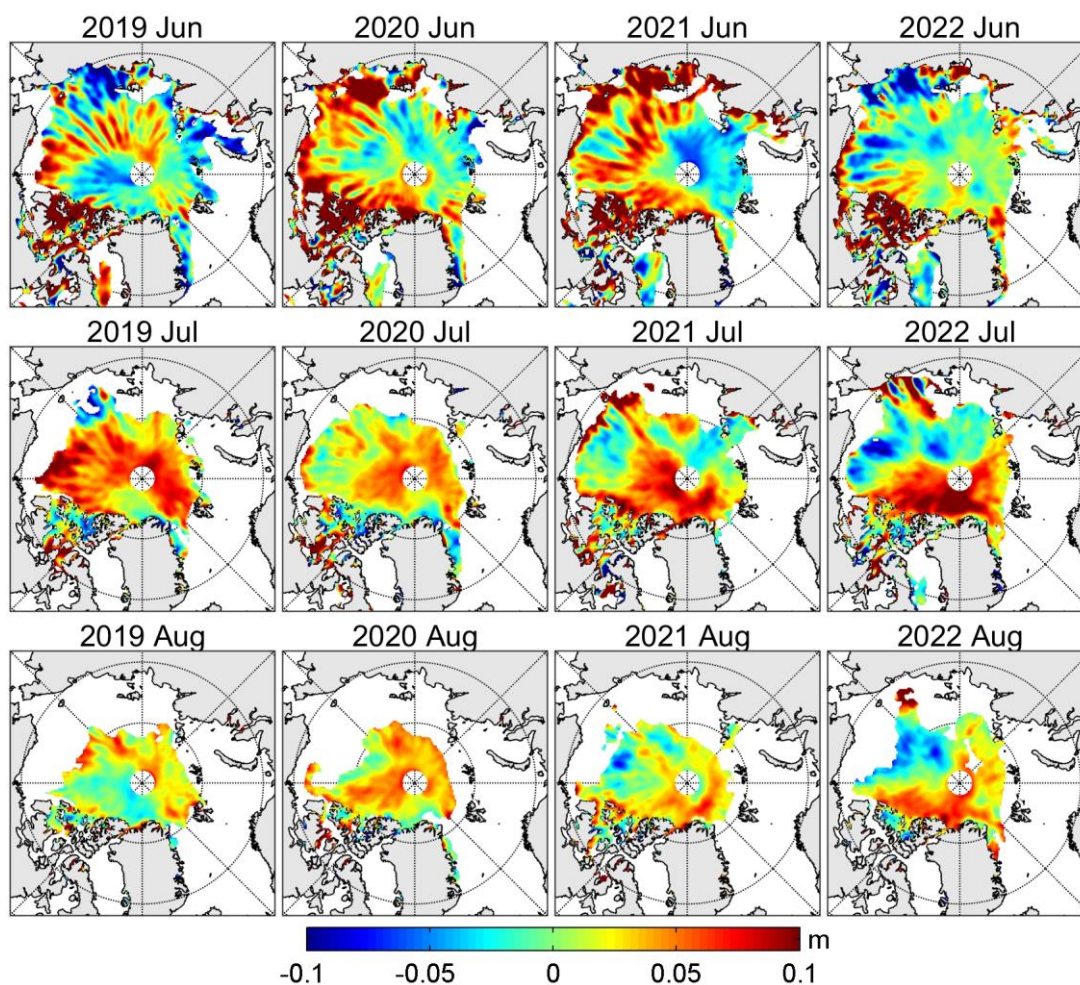

Figure 12: Mean SSHA (referenced with CI-SSH) of summer months from 2019 to 2022.

To understand the impact of melt ponds on sea surface determination, we removed the observations from June to August and
470   recalculated the MSS following the procedures described in Section 3. The MSS results and corresponding RMSE are shown
in Fig. 13(a) and (b) respectively. The dotted line in Fig. 13(b) represents the average sea-ice-covered region (determined by
sea ice concentration greater than 50%) in June-August from 2019 to 2022. The regional features shown in Fig. 13(a) are
consistent with Fig. 7(a), while decrease of SSH is clearly shown in Central Arctic in Fig. 13(b). The mean difference is -
1.0±1.47 cm inside the ice-covered region. Since the higher values from June-August are removed, the decrease is expected.
475   However, statistics shows that the impact on Summer months' data is limited. For the whole coverage in Fig. 13(b),
differences in 93.8% of the grids are within ±3 cm. In the ice-covered region, only 20.4% of the grids show SSH decreases

greater than 2 cm and the fraction is 6.3% for SSH decreases greater than 3 cm. Considering the centimetre-level RMSE of SSH (see Fig. 7(d)), the difference shown in Fig. 13(b) is not severe. It is important to note that the mean SSH results in this paper were based on monthly average sea level. Therefore, the impact of massive amount of abnormal lead observations in

480 summer months on SSH determination was limited. However, if the mean SSH were determined simply by averaging the original altimetry observations, the huge number of false leads in July and August would inevitably introduce significant biases. It is should also be noted that the number of SSH grid points in Fig. 13(a) was reduced compared with Fig. 7(a).

In summary, under the current technical conditions, the Arctic Ocean sea surface obtained by satellite altimetry from June to August is indeed greatly affected by melt ponds, and may not be able to reflect the real sea level changes in summer. This

485 needs to be especially noted in the study of seasonal changes in sea level in the sea-ice-covered Arctic Ocean. However, if appropriate calculation methods are applied, the impact of melt ponds on determining the Arctic sea surface can be alleviated.
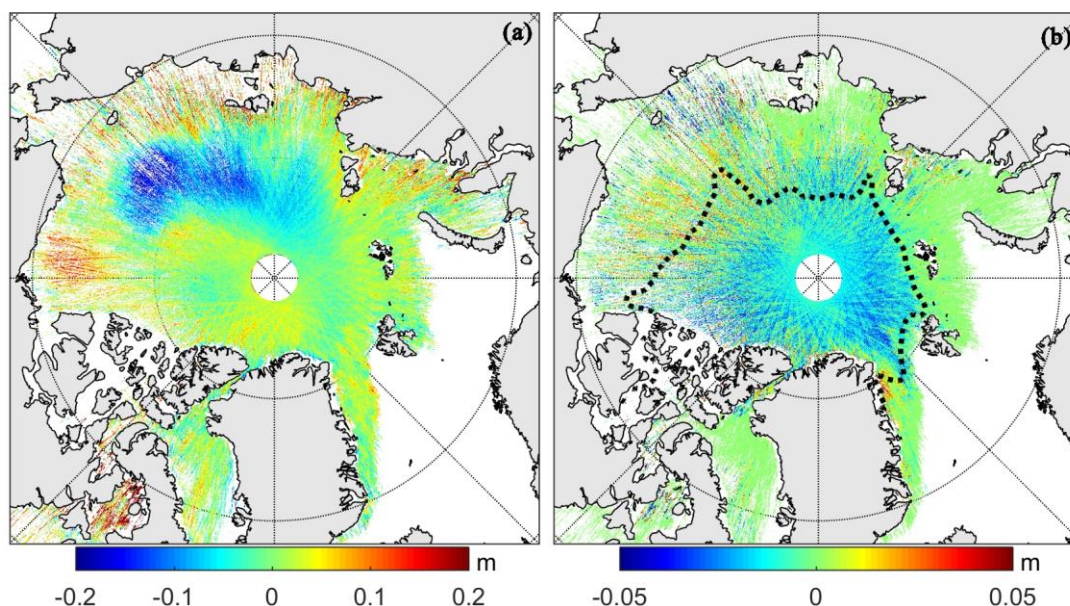

Figure 13: (a) Mean sea surface determined by combined CryoSat-2 and ICESat-2 after removing observations from June, July and August and (b) the differences compared with CI-SSHA, the dotted line indicates the average boundary of sea ice

490 **concentration beyond 50% in June-August from 2019 to 2022.**

6 Summary

In this paper, data from CryoSat-2 and ICESat-2 have been combined to determine the Arctic mean sea surface and sea level records and the results have been evaluated and discussed. The main contributions are listed as follows:

1) By comparisons of overlapping CryoSat-2 and ICESat-2 lead observations, the lead detection method of ICESat-2 ATL07

495 product are discussed. The results have shown that both strong and weak beams of ICESat-2 are consistent with CryoSat-2.

However, the classification of lead observations of ATL07 needs to be optimized, the height filtering technology is not necessary for specular leads and the amount of total lead observations is much less than expected.

2) The performances of individual CryoSat-2 and ICESat-2 data in Arctic SSH determination are compared. The two missions generally show excellent consistency with an inter-mission bias less than 1 cm. However, ICESat-2 provides sparser SSH results both in spatial and time distributions, showing the disadvantages in its current lead detection method again. Our results also suggest that ICESat-2 can achieve better precision than CryoSat-2, but it also suffers more from outliers. In general, the two missions show comparable STD of about 2 cm along 5 km ground track segments.

3) Arctic mean sea surface map, named as CI-SSH/SSHA, is determined with combined CryoSat-2 and ICESat-2 data, along with monthly and seasonally averaged SSH maps from October 2018 to October 2022. The results of combined data provide better coverage and precision than that of individual missions. Although CI-SSH/SSHA was derived with only two missions and four years' data, it shows similar accuracy compared with DTU21 and CNES_CLS 2022 MSS models in Arctic Ocean, showing the great potential of combining data from the two missions together. The time series of monthly average mean sea level derived from combined data are consistent with the results of gauge data.

4) The geophysical corrections in CryoSat-2 and ICESat-2 products are compared. Our results suggest that the ocean tide corrections should be unified when combining data from the two missions, while the differences of other corrections are negligible considering the precisions of current models.

5) The impact of summer melt ponds in Arctic sea surface determination based on satellite altimetry is also discussed. Our results show that both CryoSat-2 and ICESat-2 data are seriously contaminated by melt pond observations in June, July and August. Therefore, the altimetry derived sea levels in summer seasons are not reliable. However, it has much less impact on mean sea surface if it is calculated with monthly averaged values.

Data availability

CI-SSHA and monthly averaged sea level data presented in this manuscript can be accessed via https://www.scidb.cn/en/anonymous/VVpSbm15.

Author contribution

Chen, G. conceived and designed the methodology, analysed the data and wrote the paper. Jiang, W. supervised the entire research. Zhang, Z. , Jin, T. and Li, D. provided assistances in data analysis, visualization and paper writing.

Competing interests

The authors declare that they have no conflict of interest.

530 **References**

Andersen O. B and Piccioni G.: Recent Arctic sea level variations from satellites, Front. Mar. Sci., 3, 76, doi:10.3389/fmars.2016.00076, 2016.

Andersen, O. B., Rose, S. K., Abulaitijiang, A., Zhang, S., and Fleury, S.: The DTU21 global mean sea surface and first evaluation, Earth Syst. Sci. Data, 15, 4065–4075, doi:10.5194/essd-15-4065-2023, 2023.

535 Armitage, T. W. K., Bacon, S., Ridout, A. L., Thomas S. F., Aksenov Y., and Wingham D. J., Arctic sea surface height variability and change from satellite radar altimetry and GRACE, 2003–2014, J. Geophys. Res. Oceans, 121, 4303–4322, doi:10.1002/2015JC011579, 2021.

Bagnardi, M., Kurtz, N. T., Petty, A. A., and Kwok, R.: Sea surface height anomalies of the Arctic Ocean from ICESat-2: A first examination and comparisons with CryoSat-2, Geophys. Res. Lett., 48, e2021GL093155, 540 doi:org/10.1029/2021GL093155, 2021.

Bouzinac, C.: CryoSat product handbook, available at: https://earth.esa.int/eogateway/documents/20142/37627/cryosat-baseline-d-product-handbook/f28680ea-13de-c7e1-884a-d273b8945905?version=1.0&t=1610383270197, (last access: 15 December 2023), 2014.

Carret, A., Johannessen, J. A., Andersen, O. B., Ablain, M., Prandi, P., Blazquez, A. and Cazenave, A.: Arctic sea level 545 during the satellite altimetry era, Surv. Geophys., 38, 255-279, doi:10.1007/s10712-016-9390-2, 2017.

Chen, G., Zhang, Z., Rose, S. K., Andersen, O. B., Zhang, S. and Jin T.: A new Arctic MSS model derived from combined Cryosat-2 and ICESat observations, Int. J. Digit. Earth, 15, 2202-2222, doi:10.1080/17538947.2022.2153181, 2022.

Cheng, Y., Andersen, O. B. and Knudsen, P.: An improved 20-year Arctic Ocean altimetric sea level data record, Mar. Geod., 38, 146-162, doi:10.1080/01490419.2014.954087, 2015.

550 Connor, L. N., Laxon, S. W., Ridout, A. L., Krabill W. B. and McAdoo, D. C.: Comparison of Envisat radar and airborne laser altimeter measurements over Arctic sea ice, Remote Sens. Environ., 113, 563-570, doi:10.1016/j.rse.2008.10.015, 2009.

Dawson, G. J. and Landy, J. C.: Comparing elevation and backscatter retrievals from CryoSat-2 and ICESat-2 over Arctic summer sea ice, The Cryosphere, 17, 4165-4178, doi:10.5194/tc-17-4165-2023, 2023.

555 DiGirolamo, N. E., Parkinson, C. L., Cavalieri, D. J., Gloersen, P. and Zwally, H. J.: Sea Ice Concentrations from Nimbus-7 SMMR and DMSP SSM/I-SSMIS Passive Microwave Data, Version 2, available at: https://nsidc.org/sites/default/files/documents/user-guide/nsidc-0051-v002-userguide.pdf, (last access: 15 December 2023), 2022.

Doglioni, F., Ricker, R., Rabe B, Barth, A., Troupin, C. and Kanzow, T.: Sea surface height anomaly and geostrophic current
560 velocity from altimetry measurements over the Arctic Ocean (2011–2020), Earth Syst. Sci. Data, 15, 225-263, doi:10.5194/essd-2022-111, 2022.

Farrell, S. L., McAdoo, D. C., Laxon, S. W., Zwally, H. J., Yi, D., Ridout, A. and Giles, K.: Mean dynamic topography of the Arctic Ocean, Geophys. Res. Lett., 39, L01601, doi:10.1029/2011GL050052, 2012.

Farrell, S. L., Duncan, K., Buckley, E. M., Richter-Menge, J., and Li, R.: Mapping sea ice surface topography in high fidelity
565 with ICESat-2. Geophys. Res. Lett., 47, e2020GL090708, doi:10.1029/2020GL090708, 2020.

Forsberg, R. and Skourup, H.: Arctic Ocean gravity, geoid and sea-ice freeboard heights from ICESat and GRACE, Geophys. Res. Lett., 32, L21502, doi:10.1029/2005GL023711, 2005.

Hersbach, H., Bell, B., Berrisford, P., Hirahara, S., Horányi, A., Muñoz-Sabater, J., Nicolas, J., Peubey, C., Radu, R., Schepers, D. and Simmons, A.: The ERA5 global reanalysis. Q. J. Roy. Meteor. Soc., 146, 1999-2049, doi:
570 10.1002/qj.3803, 2020.

Jain, M., Andersen, O. B., Dall, J., and Stenseng. L,: Sea surface height determination in the Arctic using Cryosat-2 SAR data from primary peak empirical retrackers, Adv. Space Res., 55, 40-50, doi:10.1016/j.asr.2014.09.006, 2015.

Jin, T., Li, J., and Jiang, W.: The global mean sea surface model WHU2013, Geod. Geodyn., 7, 202-209, doi: 10.1016/j.geog.2016.04.006, 2016.

575 Kacimi, S. and Kwok, R.: The Antarctic sea ice cover from ICESat-2 and CryoSat-2: freeboard, snow depth, and ice thickness, The Cryosphere, 14, 4453-4474, doi:10.5194/tc-14-4453-2020, 2020.

Kim, J., Sohn, B., Lee, S., Tonboe, R. T., Kang., E. and Kim, H.: Differences between ICESat and CryoSat-2 sea ice thicknesses over the Arctic: Consequences for analyzing the ice volume trend, J. Geophys. Res. Atmos, 125, e2020JD033103, doi:10.1029/2020JD033103, 2020.

580 Kurtz, N. T., Galin, N. and Studinger, M.: An improved CryoSat-2 sea ice freeboard retrieval algorithm through the use of waveform fitting, The Cryosphere, 8, 1217-1237, doi:10.5194/tc-8-1217-2014, 2014.

Kwok, R. and Morison, J.: Dynamic topography of the ice-covered Arctic Ocean from ICESat, Geophys. Res. Lett., 38, L02501, doi:10.1029/2010GL046063, 2011.

Kwok, R., Markus, T., Kurtz, N. T., Petty, A. A., Neumann, T. A., Farrell, S. L., Cunningham, G. F., Hancock, D. W.,
585 Ivanoff, A. and Wimert, J. T.: Surface height and sea ice freeboard of the Arctic Ocean from ICESat-2: Characteristics and early results, J. Geophys. Res. Oceans, 124, 6942-6959, doi:10.1029/2019JC015486, 2019.

Kwok, R., Petty, A. A., Bagnardi, M., Kurtz N. T., Cunningham G. F., Ivanoff, A. and Kacimi, S.: Refining the sea surface identification approach for determining freeboards in the ICESat-2 sea ice products, The Cryosphere, 15, 821-833, doi: 10.5194/tc-15-821-2021, 2021a.

590   Kwok, R., Cunningham, G. F., Hancock, D. W., Ivanoff, A. and Wimert, J. T.: Ice, Cloud, and Land Elevation Satellite (ICESat-2) project: algorithm theoretical basis document (ATBD) for sea ice products (ATL07/ATL10) Release005, available at: https://nsidc.org/sites/default/files/icesat2_atl07_atl10_atl20_atl21_atbd_r005_1.pdf, (last access: 15 December 2023), 2021b.

Lawrence, I. R., Armitage, T. W. K., Tsamados, M. C., Stroeve, J. C., Dinardo, S., Ridout, A. L., Muir, A., Tilling, R. L. and
595   Shepherd, A.: Extending the Arctic sea ice freeboard and sea level record with the Sentinel-3 radar altimeters, Adv. Space Res., 68, 711-723, doi:10.1016/j.asr.2019.10.011, 2021.

Laxon, S., Peacock, N. and Smith, D.: High interannual variability of sea ice thickness in the Arctic region, Nature, 425, 947-950, doi:10.1038/nature02050, 2003.

Laxon, S. W., Giles, K. A., Ridout A. L., Wingham, D. J., Willatt, R., Cullen R., Kwok R., Schweiger, A., Zhang, J., Haas,
600   C., Hendricks, S., Krishfield, R., Kurtz, N., Farrell, S. and Davidson, M.: CryoSat-2 Estimates of Arctic Sea Ice Thickness and Volume, Geophys. Res. Lett., 40, 732–737. doi:10.1002/GRL.50193, 2013.

Lee, S., Kim, H. and Im, J.: Arctic lead detection using a waveform mixture algorithm from CryoSat-2 data, The Cryosphere, 12, 1665-1679, doi:10.5194/tc-12-1665-2018, 2018.

Lin, P., Pickart, R. S., Heorton, H., Tsamados, M., Itoh, M. and Kikuchi, T.: Recent state transition of the Arctic Ocean's
605   Beaufort Gyre, Nat. Geosc., 16, 485-491, 2023.

Lindsay, R. W. and Rothrock, D. A.: Arctic sea ice leads from advanced very high resolution radiometer images, J. Geophys. Res. Oceans, 100: 4533–4544, doi:10.1029/94JC02393, 1995.

Liu W, Jin T, Li J, et al. Adaptive Clustering-based Method for ICESat-2 Sea ice Retrieval[J]. IEEE T. Geosci. Remote, 2023, 61, 1-14, doi:10.1109/TGRS.2023.3287909, 2023.

610   Luzum, B. and Petit, G.: The IERS Conventions (2010): Reference systems and new models, Proceedings of the International Astronomical Union, 10(H16), 227-228, doi:10.1017/S1743921314005535, 2012.

Lyard, F. H., Allain, D. J., Cancet, M., Carrère, L. and Picot, N.: FES2014 global ocean tide atlas: design and performance, Ocean Sci., 17, 615-649, doi:10.5194/os-17-615-2021, 2021.

Markus, T., Neumann, T., Martino, A., Abdalati, W., Brunt, K., Csatho, B., Farrell, S., Fricker, H., Gardner, A., Harding, D.,
615   Jasinski, M., Kwok, R., Magruder, L., Lubin, D., Luthcke, S., Morison, J., Nelson, R., Neuenschwander, A., Palm, S., and Zwally, H.: The Ice, Cloud, and land Elevation Satellite-2 (ICESat-2): Science requirements, concept, and implementation, Remote Sens. Environ., 190, 260–273, https://doi.org/10.1016/j.rse.2016.12.029, 2017.

Neumann, T. A., Martino, A. J., Markus, T., Bae, S., Bock, M. R., Brenner, A. C., Brunt, K. M., Cavanaugh, J., Fernandes, S. T., Hancock, D. W., Harbeck, K., Lee, J., Kurtz, N. T., Luers, P. J., Luthcke, S. B., Magruder, L., Pennington, T. A.,
620   Ramos-Izquierdo, L., Rebold, T., Skoog, J., and Thomas, T. C.: The Ice, Cloud, and Land Elevation Satellite – 2 mission:

A global geolocated photon product derived from the Advanced Topographic Laser Altimeter System, Remote Sens. Environ., 233, 111325, https://doi.org/10.1016/j.rse.2019.111325, 2019.

Passaro, M., Rose, S. K., Andersen, O. B., Boergens, E., Calafat, F. M., Dettmering, D., and Benveniste, J.: ALES+: Adapting a homogenous ocean retracker for satellite altimetry to sea ice leads, coastal and inland waters, Remote Sens. Environ., 211: 456-471, doi:10.1016/j.rse.2018.02.074, 2018.

Peacock, N. R. and S. W. Laxon: Sea Surface Height Determination in the Arctic Ocean from ERS Altimetry, J. Geophys. Res. Oceans, 109 , C07001, doi:10.1029/2001JC001026, 2004.

Petty, A. A., Keeney, N., Cabaj, A., Kushner, P. and Bagnardi, M.: Winter Arctic sea ice thickness from ICESat-2: upgrades to freeboard and snow loading estimates and an assessment of the first three winters of data collection, The Cryosphere, 17, 127-156, doi:10.5194/tc-17-127-2023, 2023.

Poisson, J. C., Quartly, G. D., Kurekin, A. A., Thibaut, P., Hoang, Duc. And Nencioli, F.: Development of an ENVISAT altimetry processor providing sea level continuity between open ocean and Arctic leads, IEEE T. Geosci. Remote, 56, 5299-5319, doi:10.1109/TGRS.2018.2813061, 2018.

Prandi, P., Ablain, M., Cazenave, A. and Picot, N.: A new estimation of mean sea level in the Arctic Ocean from satellite altimetry[J]. Mar. Geod., 35(sup1), 61-81, doi:10.1080/01490419.2012.718222, 2012.

Prandi, P., Poisson, J. C., Faugère, Y., Guillot, A. and Dibarboure, G.: Arctic sea surface height maps from multi-altimeter combination, Earth Syst. Sci. Data, 13, 5469-5482, doi:10.5194/essd-13-5469-2021, 2021.

Quartly, G. D., Rinne, E., Passaro, M., Andersen, O. B., Dinardo, S., Fleury, S., Guillot, A., Hendricks, S., Kurekin, A. A., Müller, F. L., Ricker, R., Skourup, H. and Tsamados, M.: Retrieving sea level and freeboard in the Arctic: A review of current radar altimetry methodologies and future perspectives, Remote Sens., 11, 881, doi:10.3390/rs11070881, 2019.

Ricker, R., Hendricks, S., Helm, V., Skourup, H. and Davidson, M.: Sensitivity of CryoSat-2 Arctic sea-ice freeboard and thickness on radar-waveform interpretation, The Cryosphere, 8, 1607-1622, doi:10.5194/tc-8-1607-2014, 2014.

Ricker, R., Hendricks, S. and Beckers, J. F.: The impact of geophysical corrections on sea-ice freeboard retrieved from satellite altimetry, Remote Sens., 8, 317, doi:10.3390/rs8040317, 2014.

Rose, S. K., Andersen, O. B., Passaro, M., Ludwigsen, C. A. and Schwatke, C.: Arctic Ocean sea level record from the complete radar altimetry era: 1991–2018, Remote Sens., 11, 1672, doi:10.3390/rs11141672, 2019.

Schaeffer, P., Pujol, M. I., Veillard, P., Faugere, Y., Dagneaux, Q., Dibarboure, G. and Picot, N.: The CNES CLS 2022 Mean Sea Surface: Short Wavelength Improvements from CryoSat-2 and SARAL/AltiKa High-Sampled Altimeter Data, Remote Sens., 15, 2910, doi:10.3390/rs15112910, 2023.

Stroeve, J., Barrett, A., Serreze, M. and Schweiger, A.: Using records from submarine, aircraft and satellites to evaluate climate model simulations of Arctic sea ice thickness, The Cryosphere, 8, 1839-1854, doi:10.5194/tc-8-1839-2014, 2014.

Tilling, R., Kurtz, N. T., Bagnardi, M. Petty, A. A. and Kwok, R.: Detection of melt ponds on Arctic summer sea ice from ICESat-2, Geophys. Res. Lett., 47, e2020GL090644, doi:10.1029/2020GL090644, 2020.

Wang, Q.: Stronger variability in the Arctic Ocean induced by sea ice decline in a warming climate: Freshwater storage,

655   dynamic sea level and surface circulation, J. Geophys. Res.: Oceans, 126, e2020JC016886, doi:10.1029/2020JC016886, 2021.

Wernecke, A. and Kaleschke, L.: Lead detection in Arctic sea ice from CryoSat-2: quality assessment, lead area fraction and width distribution, The Cryosphere, 9, 1955-1968, doi:10.5194/tc-9-1955-2015, 2015.

Wingham, D. J., Francis, C. R., Baker, S., Bouzinac, C., Cullen, R., Chateau-Thierry, P., Laxon, S. W., Mallow, U.,

660   Mavrocordatos, C., Phalippou, L., Ratier, G., Rey, L., Rostan, F., Viau, P. and Wallis, D. W.: CryoSat: A mission to determine the fluctuations in Earth's land and marine ice fields, Adv. Space Res., 37, 841-871, doi:10.1016/j.asr.2005.07.027, 2006.

Xia, W. and Xie, H.: Assessing three waveform retrackers on sea ice freeboard retrieval from Cryosat-2 using Operation IceBridge Airborne altimetry datasets, Remote Sens. Environ., 204, 456-471, doi:10.1016/j.rse.2017.10.010, 2018.

665   Xiao, K., Chen, M., Wang, Q., Wang, X. and Zhang W.: Low-frequency sea level variability and impact of recent sea ice decline on the sea level trend in the Arctic Ocean from a high-resolution simulation, Ocean Dynam., 70, 787-802, doi:10.1007/s10236-020-01373-5, 2020.

Yi, D., Kurtz, N., Harbeck, J., Kwok, R., Hendricks, S. and Ricker, R.: Comparing coincident elevation and freeboard from IceBridge and five different CryoSat-2 retrackers, IEEE T. Geosci. Remote, 57, 1219-1229,

670   doi:10.1109/TGRS.2018.2865257, 2018.

Zhang, Y., Cheng, X., Liu, J. and Hui, F.: The potential of sea ice leads as a predictor for summer Arctic sea ice extent. The Cryosphere, 12, 3747-3757, doi:10.5194/tc-12-3747-2018, 2018.

Zhang, Z., Chen, G., Bo, Y., Guo, X. and Bao, J.: Performance evaluation of combining ICESat-2 and GEDI laser altimetry missions for inland lake level retrievals, Geosci. Lett., 9, 35, doi:10.1186/s40562-022-00243-w, 2022.